frontiers | Frontiers in Energy Research

TYPE Original Research
PUBLISHED 15 September 2022
DOI 10.3389/fenrg.2022.1013929

OPEN ACCESS

EDITED BY
Junfei Liang,
North University of China, China

REVIEWED BY
Tao Wang,
Southeast University, China
Chunyu Cui,
Hunan University, China

*CORRESPONDENCE
Liqing Li,
liqingli@csu.edu.cn

SPECIALTY SECTION
This article was submitted to Electrochemical Energy Conversion and Storage,
a section of the journal
Frontiers in Energy Research

RECEIVED 08 August 2022
ACCEPTED 19 August 2022
PUBLISHED 15 September 2022

CITATION
Liu Y, Gong Z and Li L (2022), Flour derived porous carbon as anode for highly robust potassium-ion batteries. *Front. Energy Res.* 10:1013929. doi: 10.3389/fenrg.2022.1013929

Flour derived porous carbon as anode for highly robust potassium-ion batteries

Yong Liu[1], Zhen Gong[2] and Liqing Li[1]*

[1]School of Energy Science and Engineering, Central South University, Changsha, China, [2]College of Life Sciences and Chemistry, Hunan University of Technology, Zhuzhou, China

Potassium-ion batteries (PIBs) have attracted increasing research interest because of the natural abundance and low cost of potassium. Nevertheless, lacking of suitable anode materials that can deliver high reversible capacity and long cycle life highly hinder the further development of PIBs. Here, we report a flour chemistry strategy to establish a porous phosphorus-doped carbon (PPDC) as anode for high-performance PIBs. The as-prepared PPDC with high hierarchically porous structure and rich P-doping not only offers fast transport of K^+ and electrons during continuous cycling, but also affords sufficient inner space to relieve volume expansion of active electrode. Therefore, the PPDC displayed high reversible capacity, excellent cyclic stability, outstanding rate performance. These results imply a great potential for applications in the field of high-energy storage devices.

KEYWORDS

flour, phosphorus-doped, porous carbon, anode, potassium-ion batteries, high performance

1 Introduction

It is of great significance to design energy storage systems with the merits of low cost, eco-friendliness, long cycle and high energy density. (Zhou et al., 2015; Tan et al., 2016; Zhang et al., 2018; Zhao et al., 2018; Wu et al., 2019a; Gao et al., 2019; Sun et al., 2019; Cui et al., 2020; Liu et al., 2020; Wu et al., 2020; Guo et al., 2021; Liu et al., 2021; Pfleging, 2021; Wang et al., 2022a; Wang et al., 2022b; Huang et al., 2022; Xiao et al., 2022; Zhang et al., 2022; Zhong et al., 2022) Potassium-ion batteries (PIBs) have been considered as a superior alternative to lithium-ion batteries, due to abundant storage (2.09 wt% vs. 0.0017 wt% for Li) in the earth's crust, and lower redox potential of K/K^+ (-2.93 V vs.-2.71 V for Na^+/Na) that leads to a wider potential window and a higher energy density. (Zhou et al., 2015; Tan et al., 2016; Zhao et al., 2018; Gao et al., 2019; Cui et al., 2020; Liu et al., 2020; Pfleging, 2021; Wang et al., 2022b; Li et al., 2022) Nevertheless, larger radius of K^+ (1.38 Å) compared with that of Li^+ and Na^+ gives rise to huge volume expansion of the electrode material during charge/discharge, which greatly limits the range of available electrode materials. (Liu et al., 2018; Zhao et al., 2018; Liu et al., 2020; Deng et al., 2021; Pfleging, 2021; Wang et al., 2022b; Li et al., 2022).

In order to achieve high-performance PIBs, it is important to select suitable anode materials. To date, various materials have been explored as potential anode candidates for

PIBs, including carbon materials, metal oxides, metal sulfides, phosphides, MXene based materials. (Wang et al., 2018; Zhang et al., 2019a; Wu et al., 2019b; Chen et al., 2020; Li et al., 2020; Cao et al., 2021; Deng et al., 2021; Li et al., 2021; Luo et al., 2021; Zhang et al., 2021; Cao et al., 2022). Among them, carbon-based materials present great potential toward commercialization due to their abundant reserve, low prices and excellent electrochemical properties. For instance, Zhu reported a completely opening radial pores in N/O dual-doped carbon nanospheres (RPCNSs) as anode for high-power PIBs. The RPCNS with hierarchical structure and N/O dual-doping permits speedy ions and electrons transportation within the carbon nanospheres anode, thus achieving a reversible capacity and long-term cycling life over 2000 cycles. (Deng et al., 2021).

It is worth noting that heteroatom doping such as B, N, O, P, and S is an effective strategy to enhance the physicochemical property of carbon matrix. (Liu et al., 2017; Song et al., 2017; Chang et al., 2018; Cao et al., 2020; Fang et al., 2021; Cao et al., 2022) On the one hand, heteroatom doping is efficient in introducing defects in carbon materials, and further provide more active sites for K^+ storage. (Zeng et al., 2014; Yao et al., 2021; Zhou et al., 2021) On the other hand, the doping elements can also increase the conductivity, expand the interlayer distance of carbon based materials, thus imparting outstanding electrochemical performance to the carbon materials. (Zeng et al., 2014; Liu et al., 2017; Song et al., 2017; Chang et al., 2018; Cao et al., 2020; Fang et al., 2021; Yao et al., 2021; Zhou et al., 2021; Cao et al., 2022).

Here, a porous phosphorus-doped carbon (PPDC) was designed as high-performance anode for PIBs. The constructed PPDC with hierarchically porous structure and rich P-doping facilitates excellent electronic/ionic conductivity, offers effective remission of the mechanical stress during potassiation/depotassiation, thus affording exceptional performance of the PPDC electrode. As a result, the obtained PPDC could display a high reversible capacity of 292 mA h g^{-1} at 100 mA g^{-1} after continuous 80 cycles, remarkable rate capabilities (377、321、248、198、182、136、93 mA h g^{-1} at 0.1, 0.2, 0.3, 0.4, 0.5, 1.0, and 2.0 A g^{-1}), indicating show great application prospects in the field of high-performance PIBs.

2 Experimental section

2.1 Preparation of the porous phosphorus-doped carbon (PPDC)

The synthesis method of the PPDC samples used in this study is as follows. First, phosphoric acid (10 mL, 87%) was diluted into a 10% concentration phosphoric acid solution. The flour was dissolved in 50 mL, 10% phosphoric acid solution to form a homogeneous gel-like substance. The flour was purchased from a ordinary vegetable market. Then, the gel was reacted in a reactor at 180°C for 12 h. The obtained samples after the reaction were dried and heated to 600, 700, and 800°Cunder argon flow at a heating rate of 3°C min^{-1} for 3 h. Finally, the calcined samples were washed with 10% HCl aqueous solution, filtered, and washed with distilled water several times until neutral; the porous carbon with different heating temperatures were dried at 60°C for 12 h and marked as PPDC-600, PPDC- 700 and PPDC-800. Using cheap flour as raw material, PPDC with hierarchical porous structure and phosphorus element doping was designed as an anode material for k-ion half-cells. The high specific surface area, hierarchical porous structure, and phosphorus doping of PPDC materials can facilitate ion/electron transport during charge and discharge.

2.2 Material characterizations

Raman spectra were tested with a 488 nm laser (Jobin-Yvon Lab RAM HR-800) and thermal gravimetric analysis (TGA) was performed with a TG-209F1. N_2 adsorption/desorption isotherm was carried out specific surface area and porosity distribution measurement with an Autosorb IQ Gas Sorption System at 77 K. The morphologies and chemical structures of the carbonaceous material were characterized by SEM (Zeiss SIGMA).

2.3 Electrochemical characterizations

Active materials, conductive carbon and carboxymethyl cellulose with mass ratio of 8:1:1 were dispersed in a mixed solution (1 mL) of ethanol and H_2O, and ball-milled for 30 min. Then, the obtained slurries were painted on the Cu foil and dried at vacuum environment at 60°C for 12 h. The working electrode with an average mass loading of each electrode about 0.9 mg cm^{-2} is a disc with diameter of 12 mm. Potassium metal and glass fiber film were used as the anode electrode and the separator, respectively. The 5 M KFSI dissolved in ethylene carbonate/dimethyl carbonate mixture (EC/DMC by 1:1 vol.) was used as electrolyte. The coin-type cells (2032) were assembled in a MB-Labstar (1,200/780) glove box (Munich, Germany) under Ar atmosphere. The concentrations of moisture and oxygen were maintained below 0.5 ppm. The CT2001A battery test system (LANDTE Co., China) and a CHI660E electrochemical station (CHI instrument Co., Shanghai, China) were used to test the electrochemical performance.

3 Results and discussions

3.1 Morphological characterizations

The micromorphology of obtained PPDC-600, PPDC-700 and PPDC-800 were investigated by scanning electron

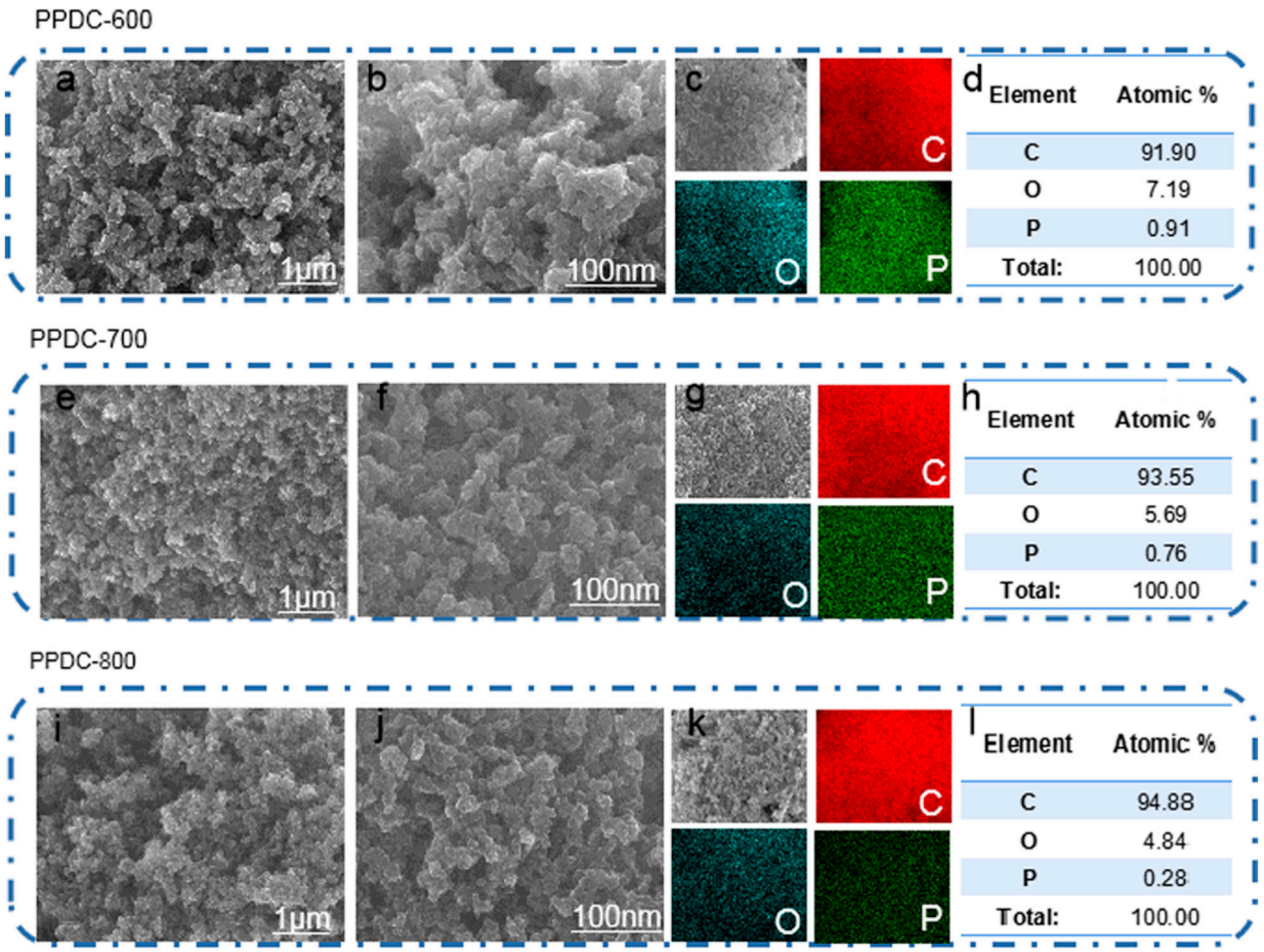

FIGURE 1
Morphological and structural characterizations. **(A,B)** SEM images of PPDC-600 electrode at different magnifications; **(C)** Element mapping of C, O and P for PPDC-600; **(D)** Element content statistics of PPDC-600; **(E,F)** SEM images of PPDC-700 electrode at different magnifications; **(G)** Element mapping of C, O and P for PPDC-700; **(H)** Element content statistics of PPDC-700; **(I,J)** SEM images of PPDC-800 electrode at different magnifications; **(K)** Element mapping of C, O and P for PPDC-800; **(L)** Element content statistics of PPDC-800.

microscope (SEM) images and SEM-mapping (Figure 1). As shown in Figures 1A,B, the PPDC-600 exhibited typical porous structure with rough surface and conductive network. This structure beneficial to achieve fast ion/electron transportation path during charge and discharge process. Figure 1C is element mapping of C, O and P for PPDC-600. Obviously, the C, O and P element evenly distribute in the carbon skeleton. Figure 1 d displays the element content statistics of C, O and P in PPDC-600. What is noteworthy is that the P doping is conductive to provide more active sites for K^+ storage and further enhance the electrical conductivity, thus offering excellent battery performance. Figure 1E-l demonstrate similar porous structure and uniform distribution of C, O and P in PPDC-600, PPDC-700 and PPDC-800. The difference is the element contents of C, O and P due to different calcination temperatures.

3.2 Structural characterizations

Raman spectroscopy measurements were used to characterize the structures of PPDC-600, PPDC-700, PPDC-800 (Figures 2A–C). Apparently, two obvious Raman peaks for the three samples appearing at about 1,350 cm^{-1} and 1,600 cm^{-1} are assigned to the D band of amorphous carbon and G band of graphitic carbon, respectively. Obviously, the values of I_D:I_G ratio of the PPDC gradually decrease as the temperature rises, indicating the increasing degree of graphitization, the reductive ordered carbon atoms and active sites (Zeng et al., 2014; Yao et al., 2021; Zhou et al., 2021). All in all, temperature is a double-edged sword. The PPDC-700 were prepared at an appropriate temperature of 700°C, thus displayed better K+ storage performance than PPDC-600 and PPDC-800. Nitrogen adsorption and desorption isotherms and pore size distribution were analyzed to investigate the

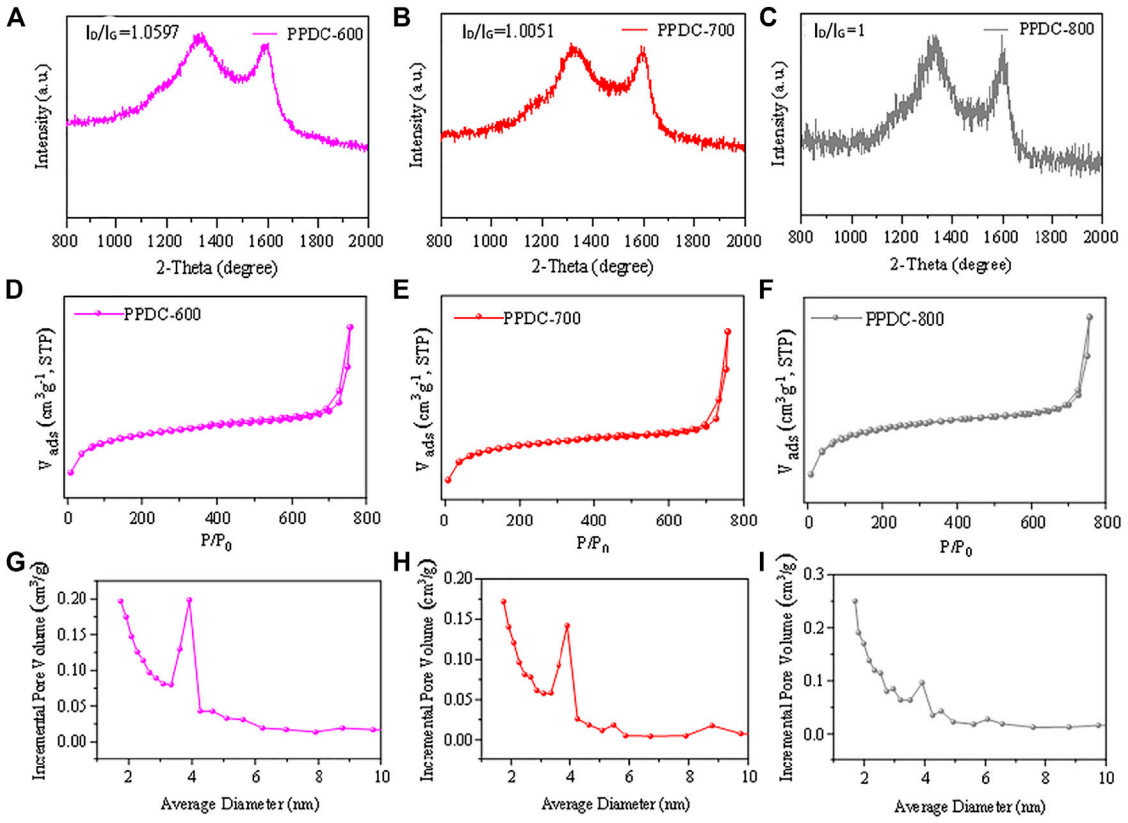

FIGURE 2
Structural and compositional information. **(A,B,C)** Raman spectra for PPDC-600, PPDC-700, PPDC-800, respectively; **(D,E,F)** N_2 adsorption-desorption isotherms for PPDC-600, PPDC-700, PPDC-800, respectively; **(G,H,I)** the corresponding pore size distribution.

microporous and mesoporous structures of the PPDC. As displayed in Figures 2D–F, specific surface areas of the PPDC-600, PPDC-700, PPDC-800 are calculated to be 765, 796, and 806 $m^2 g^{-1}$ Figures 2G–I exhibit that the pores mainly locates between 2 nm and 10 nm, indicating the existence of mesoporous. The large specific surface area and hierarchically porous structure are beneficial to effectively accommodate potassium ion storage and alleviate volume expansion. (Song et al., 2017; Zhang et al., 2019b; Zhou et al., 2020).

3.3 Battery performance characterizations

The electrochemical performance of as-prepared three samples (PPDC-600, PPDC-700 and PPDC-800) were investigated to explore the influence of carbonization temperature. Figure 3A and Supplementary Figure S1 are the charge–discharge voltage profiles for selected cycles of PPDC anodes at a current density 100 mA g^{-1}, demonstrating similar battery behavior of the PPDC-600, PPDC-700 and PPDC-800 electrodes. As shown in Figure 3B and Supplementary Figure S2, the cyclic performances of PPDC electrodes were further tested at 100 mA g^{-1}. The Coulombic efficiency experiences a jitter at about 18th cycle, and dive in the last cycle, due to sudden changes in ambient temperature. The PPDC-700 delivers a initial discharge capacities of 565 mA h g^{-1} and charge capacities of 376 mA h g^{-1} and maintains a higher reversible capacity of 310 mA h g^{-1} after continuous 50 cycles, indicating that the PPDC-700 displays higher reversible capacity and better cyclic stability. The initial large discharge capacity phenomenon is attributed to the SEI formed on the anode. The higher reversible capacity of the PPDC-700 was also proved by the larger peak area of the PPDC-700 than that of the PPDC-600 and PPDC-800 at 1 mV s^{-1} (Supplementary Figure S3). Figure 3C presents that the essentially unchanged shape of the charge/discharge curves of the PPDC-700 anode at increased current densities, suggesting the prominent reaction kinetics of K-ions intercalation/deintercalation. Figure 3D describes the rate performances of the PPDC-600, PPDC-700 and PPDC-800 at different current densities form 100 mA g^{-1} to 2 A g^{-1}. The PPDC-700 electrode shows the higher rate capacities of 377、321、248、198、182、136、93 mA h g^{-1} at 0.1, 0.2, 0.3,0.4, 0.5, 1.0, and 2.0 A g^{-1}, respectively. The high invertible capacity of

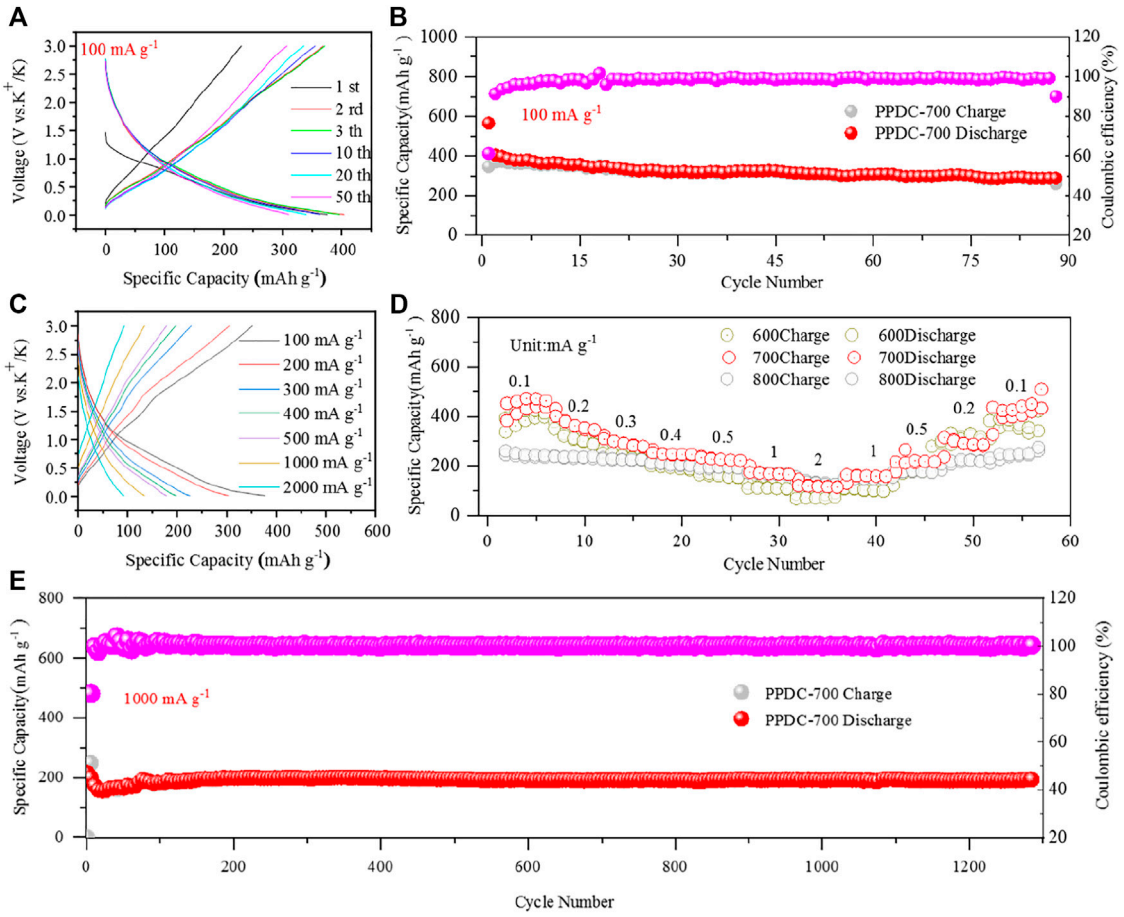

FIGURE 3
(A) Charge–discharge voltage profiles for selected cycles of the PPDC-700 anode at a current density of 100 mA g^{-1}; **(B)** Cyclic performances of the PPDC-700 anode at 100 mA g^{-1}; **(C)** Charge–discharge voltage profiles of the PPDC-700 electrode at different current densities; **(D)** Rate capability of the PPDC-600, PPDC-700 and PPDC-800 anodes at different current densities; **(E)** Cyclic performances of PPDC-700 anode at 1,000 mA g^{-1}.

377 mA h g^{-1} is still obtained when the current density returns to 100 mA g^{-1} Figure 3C exhibits the long-cycle of PPDC-700 electrode at 1,000 mA g^{-1}. After 1,000 cycles, the PPDC-700 always keeps a specific capacity as high as 197 mA h g^{-1} while maintaining close to 100% Coulombic efficiency. It is proved that the hierarchically porous structure, and appropriate graphitization degree and P-doping content of the PPDC-700 electrode provide fast ion/electron transportation and effectively relieve the mechanical stress during the cycle to enhance the battery performance.

3.4 Kinetic analysis

CV curves was measured at scan rates of 0.1–10 mV s^{-1} in a voltage range from 0.01 to 3 V to analyze the kinetic mechanism of the PPDC-600, PPDC-700 and PPDC-800 electrodes (Figure 4). Figures 4A–C display similar the changing trend of peak shape for the PPDC-600, PPDC-700 and PPDC-800 electrodes. Figures 4D–F manifest the separation of the capacitive contribution (inner region) from the total capacity (outer region). The capacitive capacities of the PPDC-600, PPDC-700 and PPDC-800 electrodes account for 39.5%, 48.7% and 50.1% at a low scan rate of 1 mV s^{-1}, indicating the charge storage behavior is dominated by the ionic diffusion and surface reaction process. As presented in Figures 4G–I, with the scan rate rising to 0.1, 0.5, 1, 2, 5 and 10 mV s^{-1}, the fraction of capacitive capacity for the PPDC-700 increases to 31.8%, 39.9%, 48.7%, 52.5%, 77.1% and 98.9%, respectively. As for the PPDC-600, the fraction of capacitive capacity increases to 38.4%, 45.6%, 52.4%, 59.7%, 75.6%, and 96.8%, respectively. For the PPDC-800, the fraction of capacitive capacity increases to 35.8%, 44.4%,

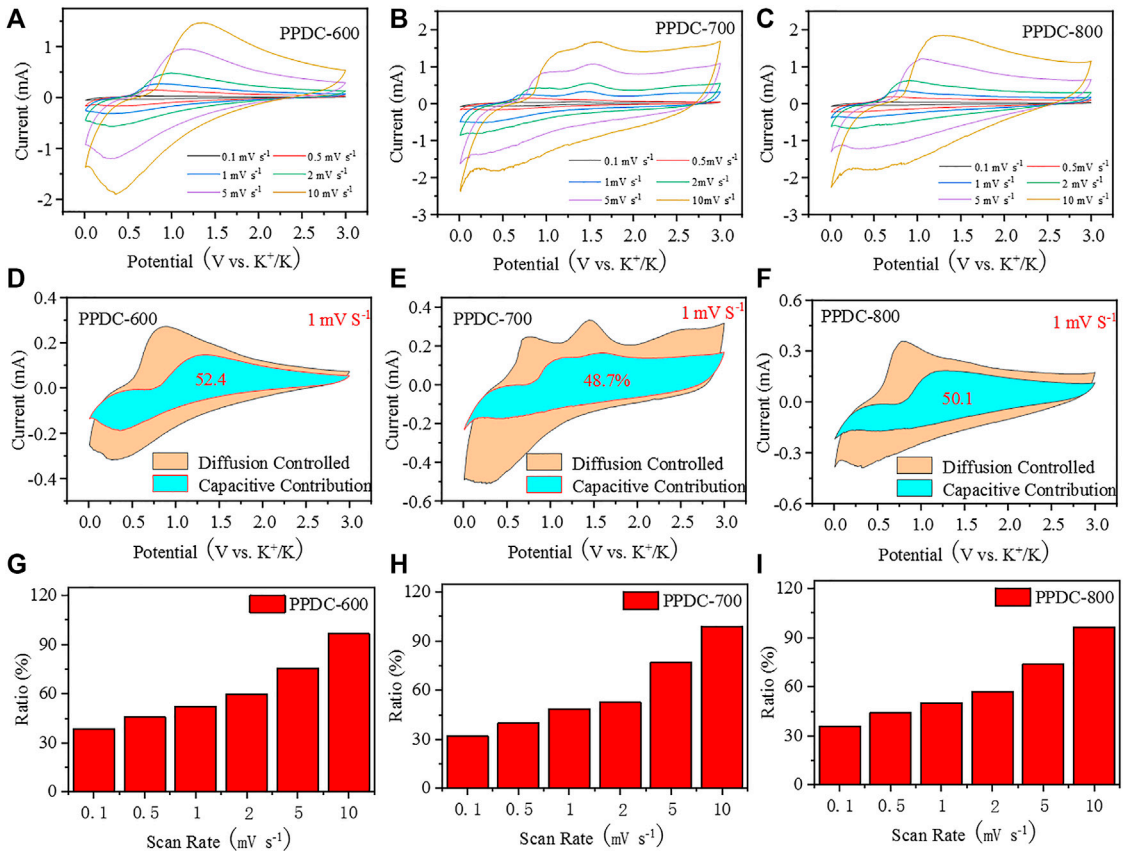

FIGURE 4
Kinetic analysis of the PPDC electrodes. CV curves of **(A)** the PPDC-600, **(B)** the PPDC-700 and **(C)** the PPDC-800 at various scan rates of 0.1–10 mV s^{-1}; Contribution of the surface process at scan rate of 1 mV s^{-1} in **(D)** the PPDC-600, **(E)** the PPDC-700 and **(F)** the PPDC-800; Contribution of the surface process in **(G)** the PPDC-600, **(H)** the PPDC-700 and **(I)** the PPDC-800 at different scan rates.

50.1%, 57.2%, 73.9% and 96.4%, respectively (Supplementary Figure S4). This phenomenon further confirmed that PPDC-700 anode for PIBs with superior electrochemical reaction kinetics, thus provides higher reversible capacity, better cyclic stability and rate performance.

4 Conclusion

In summary, a porous phosphorus-doped carbon was prepared as anode for high-performance PIBs. This porous structure and P-doping have the following benefits: 1) the hierarchically porous structure with high specific surface area effectively relieves the mechanical stress during potassiation/depotassiation, thus affording exceptional cyclic stability of the PPDC electrode; 2) the rich P-doping carbon matrix facilitates excellent electronic/ionic conductivity, achieving favorable electrochemical reaction kinetics. Therefore, the PPDC electrode presented high specific capacity, outstanding cyclic performance and rate performance. The work gives some guidance for rational design of biocarbon anode for high-performance PIBs.

5 Equations

The equations should be inserted in from the equation editor.

$$f(x) = a_0 + \sum_{n=1}^{\infty}\left(a_n \cos\frac{n\pi x}{L} + b_n \sin\frac{n\pi x}{L}\right)$$

6 Nomenclature

6.1 Resource identification initiative

To take part in the Resource Identification Initiative, please use the corresponding catalog number and RRID in your current manuscript. For more information about the project and for steps on how to search for an RRID, please click here.

6.2 Life science identifiers

Life Science Identifiers (LSIDs) for ZOOBANK registered names or nomenclatural acts should be listed in the manuscript before the keywords with the following format:

urn:lsid:<Authority>:<Namespace>:<ObjectID>[:<Version>]

For more information on LSIDs please see Inclusion of Zoological Nomenclature section of the guidelines.

Data availability statement

The original contributions presented in the study are included in the article/Supplementary Material, further inquiries can be directed to the corresponding author.

Author contributions

YL: Conceptualization, methodology, and writing—original draft; ZG: Consulting and collecting literatures; LL: Checking manuscript.

Conflict of interest

The authors declare that the research was conducted in the absence of any commercial or financial relationships that could be construed as a potential conflict of interest.

Publisher's note

All claims expressed in this article are solely those of the authors and do not necessarily represent those of their affiliated organizations, or those of the publisher, the editors and the reviewers. Any product that may be evaluated in this article, or claim that may be made by its manufacturer, is not guaranteed or endorsed by the publisher.

Supplementary material

The Supplementary Material for this article can be found online at: https://www.frontiersin.org/articles/10.3389/fenrg.2022.1013929/full#supplementary-material

References

Cao, G. Q., Bi, D., Zhao, J. X., Zheng, J., Wang, Z. K., Lai, Q. X., et al. (2020). Transformation of ZIF-8 nanoparticles into 3D nitrogen-doped hierarchically porous carbon for Li-S batteries. *RSC Adv.* 10 (29), 17345–17352. doi:10.1039/C9RA10063F

Cao, J. H., Xu, H. J., Zhong, J., Li, X. Q., Li, S. Y., Wang, Y. Y., et al. (2021). Dual-carbon electrode-based high-energy-density potassium-ion hybrid capacitor. *ACS Appl. Mat. Interfaces* 13 (7), 8497–8506. doi:10.1021/acsami.1c00115

Cao, J. H., Zhong, J., Xu, H. J., Li, S. Y., Deng, H. L., Wang, T., et al. (2022). N/S co-doped carbon nanosheet bundles as high-capacity anode for potassium-ion battery. *Nano Res.* 15 (3), 2040–2046. doi:10.1007/s12274-021-3773-5

Chang, Z., Ding, B., Dou, H., Wang, J., Xu, G. Y., and Zhang, X. G. (2018). Hierarchically porous multilayered carbon barriers for high-performance Li–S batteries. *Chem. Eur. J.* 24 (15), 3768–3775. doi:10.1002/chem.201704757

Chen, M. X., Wang, L., Sheng, X. H., Wang, T., Zhou, J., Li, S., et al. (2020). An ultrastable nonaqueous potassium-ion hybrid capacitor. *Adv. Funct. Mat.* 30 (40), 2004247. doi:10.1002/adfm.202004247

Cui, G. L., Li, G. R., Luo, D., Zhang, Y. G., Zhao, Y., Wang, D. R., et al. (2020). Three-dimensionally ordered macro-microporous metal organic frameworks with strong sulfur immobilization and catalyzation for high-performance lithium-sulfur batteries. *Nano Energy* 72, 104685. doi:10.1016/j.nanoen.2020.104685

Deng, H. L., Wang, L., Li, S. Y., Zhang, M., Wang, T., Zhou, J., et al. (2021). Radial pores in nitrogen/oxygen dual-doped carbon nanospheres anode boost high-power and ultrastable potassium-ion batteries. *Adv. Funct. Mat.* 31 (51), 2107246. doi:10.1002/adfm.202107246

Fang, X. Z., Jiang, Y., Zhang, K. L., Hu, G., and Hu, W. W. (2021). MOF-derived fluorine and nitrogen co-doped porous carbon for an integrated membrane in lithium-sulfur batteries. *New J. Chem.* 45, 2361–2365. doi:10.1039/d0nj05912a

Gao, C., Fang, C. Z., Zhao, H. M., Yang, J. Y., Gu, Z. D., Sun, W., et al. (2019). Rational design of multi-functional CoS@rGO composite for performance enhanced Li-S cathode. *J. Power Sources* 421, 132–138. doi:10.1016/j.jpowsour.2019.03.015

Guo, J., Jiang, H. L., Li, X. C., Chu, Z., Zheng, W. J., Dai, Y., et al. (2021). Defective graphene coating-induced exposed interfaces on CoS nanosheets for high redox electrocatalysis in lithium-sulfur batteries. *Energy Storage Mat.* 40, 358–367. doi:10.1016/j.ensm.2021.05.03

Huang, T. L., Cao, Q., Jing, B., Wang, X. Y., Wang, D., and Liang, L. B. (2022). Towards high performance lithium-sulfur battery: Investigation on the capability of metalloid to regulate polysulfides. *Chem. Eng. J.* 430 (1), 132677. doi:10.1016/j.cej.2021.132677

Li, X. Q., Chen, M. X., Wang, L., Xu, H. J., Zhong, J., Zhang, M., et al. (2020). Nitrogen-doped carbon nanotubes as an anode for a highly robust potassium-ion hybrid capacitor. *Nanoscale Horiz.* 5 (12), 1586–1595. doi:10.1039/D0NH00451K

Li, S. Y., Deng, H. L., Chu, Z. L., Wang, T., Wang, L., Zhang, Q., et al. (2021). Fast-Charging nonaqueous potassium-ion batteries enabled by rational construction of oxygen-rich porous nanofiber anodes. *ACS Appl. Mat. Interfaces* 13 (42), 50005–50016. doi:10.1021/acsami.1c15524

Li, S., Cao, J., Wang, T., Wang, L., Deng, H., Zhang, Q., et al. (2022). Intercalation and covalent bonding strategies for constructing a stable cathode for high-energy density and long-cycling potassium-organic batteries. *Chem. Eng. J.* 431, 133215. doi:10.1016/j.cej.2021.133215

Liu, Y. Z., Li, G. R., Chen, Z. W., and Peng, X. S. (2017). CNT-threaded N-doped porous carbon film as binder-free electrode for high-capacity supercapacitor and Li-S battery. *J. Mat. Chem. A* 5 (20), 9775–9784. doi:10.1039/c7ta01526g

Liu, D., Huang, X., Qu, D., Zheng, D., Wang, G., Harris, J., et al. (2018). Confined phosphorus in carbon nanotube-backboned mesoporous carbon as superior anode material for sodium/potassium-ion batteries. *Nano Energy* 52, 1–10. doi:10.1016/j.nanoen.2018.07.023

Liu, H. Z., Zhang, G. H., Zheng, X., Chen, F. J., and Duan, H. G. (2020). Emerging miniaturized energy storage devices for microsystem applications: from design to integration. *Int. J. Extrem. Manuf.* 2, 042001. doi:10.1088/2631-7990/abba12

Liu, Y. T., Liu, S., Li, G. R., Gao, X. P., and Gao, X. P. (2021). Strategy of enhancing the volumetric energy density for lithium-sulfur batteries. *Adv. Mat.* 33 (8), 2003955. doi:10.1002/adma.202003955

Luo, H. Y., Chen, M. X., Cao, J. H., Zhang, M., Tan, S., Wang, L., et al. (2021). Cocoon silk-derived, hierarchically porous carbon as anode for highly robust potassium-ion hybrid capacitors. *Nano-Micro Lett.* 12 (1), 113–13. doi:10.1007/s40820-020-00454-w

Pfleging, W. (2021). Recent progress in laser texturing of battery materials: a review of tuning electrochemical performances, related material development, and prospects for large-scale manufacturing. *Int. J. Extrem. Manuf.* 3, 012002. doi:10.1088/2631-7990/abca84

Song, X., Wang, S. Q., Bao, Y., Liu, G. X., Sun, W. P., Ding, L. X., et al. (2017). A high strength, free-standing cathode constructed by regulating graphitization and

the pore structure in nitrogen-doped carbon nanofibers for flexible lithium–sulfur batteries. *J. Mat. Chem. A* 5 (15), 6832–6839. doi:10.1039/c7ta01171g

Sun, H. T., Zhu, J., Baumann, D., Peng, L. L., Xu, Y. X., Shakir, I., et al. (2019). Hierarchical 3D electrodes for electrochemical energy storage. *Nat. Rev. Mat.* 4 (1), 45–60. doi:10.1038/s41578-018-0069-9

Tan, Y. B., Jia, Z. Q., Lou, P. L., Cui, Z. H., and Guo, X. X. (2016). Self-assembly sandwiches of reduced graphene oxide layers with zeolitic-imidazolate-frameworks-derived mesoporous carbons as polysulfides reservoirs for lithium-sulfur batteries. *J. Power Sources* 341, 68–74. doi:10.1016/j.jpowsour.2016.11.114

Wang, G., Xiong, X. H., Xie, D., Lin, Z. H., Zheng, J., Zheng, F. H., et al. (2018). Chemically activated hollow carbon nanospheres as a high-performance anode material for potassium ion batteries. *J. Mat. Chem. A* 6, 24317–24323. doi:10.1039/c8ta09751h

Wang, L., Wang, T., Peng, L. L., Wang, Y. L., Zhang, M., Zhou, J., et al. (2022). The promises, challenges and pathways to room-temperature sodium-sulfur batteries. *Natl. Sci. Rev.* 9 (3), nwab050. doi:10.1093/nsr/nwab050

Wang, Y. Y., Guo, Y., Zhong, J., Wang, M., Wang, L., Li, S. Y., et al. (2022). *In situ* formation of lithiophilic $Li_{22}Sn_5$ alloy and high Li-ion conductive Li_2S/Li_2Se via metal chalcogenide SnSSe for dendrite-free Li metal anodes. *J. Energy Chem.* 73, 339–347. doi:10.1016/j.jechem.2022.06.039

Wu, Q. P., Zhou, X. J., Xu, J., Cao, F. H., and Li, C. L. (2019). Carbon-based derivatives from metal-organic frameworks as cathode hosts for Li–S batteries. *J. Energy Chem.* 28 (11), 94–113. doi:10.1016/j.jechem.2019.01.005

Wu, Y., Hu, S. H., Xu, S., Wang, J. W., Peng, Z. Q., Zhang, Q. B., et al. (2019). Boosting potassium-ion battery performance by encapsulating red phosphorus in free-standing nitrogen-doped porous hollow carbon nanofibers. *Nano Lett.* 19 (2), 1351–1358. doi:10.1021/acs.nanolett.8b04957

Wu, Z. L., Wang, L., Chen, S. X., Zhu, X. M., Deng, Q., Wang, J., et al. (2020). Facile and low-temperature strategy to prepare hollow ZIF-8/CNT polyhedrons as high-performance lithium-sulfur cathodes. *Chem. Eng. J.* 404, 126579. doi:10.1016/j.cej.2020.126579

Xiao, M., Li, R. X., Yang, T., and Dai, Y. (2022). The progress and perspective of electrospun carbon nanofibers based anode materials for potassium ion storage: A mini review. *Front. Energy Res.* 10, 966825. doi:10.3389/fenrg.2022.966825

Yao, S. S., He, Y. P., Wang, Y. Q., Bi, M. Z., Liang, Y. Z., Majeed, A., et al. (2021). Porous N-doped carbon nanofibers assembled with nickel ferrite nanoparticles as efficient chemical anchors and polysulfide conversion catalyst for lithium-sulfur batteries. *J. Colloid Interface Sci.* 601, 209–219. doi:10.1016/j.jcis.2021.05.125

Zeng, L. C., Pan, F. S., Li, W. H., Jiang, Y., Zhong, X. W., and Yu, Y. (2014). Free-standing porous carbon nanofibers-sulfur composite for flexible Li-S battery cathode. *Nanoscale* 6 (16), 9579–9587. doi:10.1039/c4nr02498b

Zhang, A. Y., Fang, X., Shen, C. F., Liu, Y. H., Seo, I. G., Ma, Y. Q., et al. (2018). Functional interlayer of PVDF-HFP and carbon nanofiber for long-life lithium-sulfur batteries. *Nano Res.* 11 (6), 3340–3352. doi:10.1007/s12274-017-1929-0

Zhang, M., Shoaib, M., Fei, H. L., Wang, T., Zhong, J., Fan, L., et al. (2019). Hierarchically porous N-doped carbon fibers as a free-standing anode for high-capacity potassium-based dual-ion battery. *Adv. Energy Mat.* 9 (37), 1901663. doi:10.1002/aenm.201901663

Zhang, M., Wei, Z., Wang, T., Muhammad, S., Zhou, J., Liu, J., et al. (2019). Nickel-iron layered double hydroxides and reduced graphene oxide composite with robust lithium ion adsorption ability for high-capacity energy storage systems. *Electrochimica Acta* 296, 190–197. doi:10.1016/j.electacta.2018.11.058

Zhang, M., Zhong, J., Kong, W. Q., Wang, L., Wang, T., Fei, H. L., et al. (2021). A high capacity and working voltage potassium-based dual ion batteries. *Energy & Environ. Mater.* 4 (3), 413–420. doi:10.1002/eem2.12086

Zhang, M., He, Y. X., Xu, H. J., Ma, C., Liang, J. F., Wang, Y. Y., et al. (2022). Nb_2O_5 nanoparticles embedding in graphite hybrid as a high-rate and long-cycle anode for lithium-ion batteries. *Rare Met.* 41 (3), 814–821. doi:10.1007/s12598-021-01863-5

Zhao, X. H., Kim, M., Liu, Y., Ahn, H. J., Kim, K. W., Cho, K. K., et al. (2018). Root-like porous carbon nanofibers with high sulfur loading enabling superior areal capacity of lithium sulfur batteries. *Carbon* 128, 138–146. doi:10.1016/j.carbon.2017.11.025

Zhong, J., Wang, T., Wang, L., Peng, L. L., Fu, S. B., Zhang, M., et al. (2022). A silicon monoxide lithium-ion battery anode with utrahigh areal capacity. *Nano-Micro Lett.* 14, 50. doi:10.1007/s40820-022-00790-z

Zhou, J. W., Yu, X. S., Fan, X. X., Wang, X. J., Li, H. W., Zhang, Y. Y., et al. (2015). The impact of the particle size of a metal–organic framework for sulfur storage in Li–S batteries. *J. Mat. Chem. A* 3 (16), 8272–8275. doi:10.1039/c5ta00524h

Zhou, J., Chen, M. X., Wang, T., Li, S. Y., Zhang, Q. S., Zhang, M., et al. (2020). Covalent selenium embedded in hierarchical carbon nanofibers for ultra-high areal capacity Li-Se batteries. *iScience* 23 (3), 100919. doi:10.1016/j.isci.2020.100919

Zhou, N., Dong, W. D., Zhang, Y. J., Wang, D., Wu, L., Wang, L., et al. (2021). Embedding tin disulfide nanoparticles in two-dimensional porous carbon nanosheet interlayers for fast-charging lithium-sulfur batteries. *Sci. China Mat.* 61 (11), 2697–2709. doi:10.1007/s40843-021-1669-9